

Potential improvements of landslide prediction by hydro-meteorological thresholds: an investigation based on reanalysis soil moisture data and principal component analysis

Nunziarita Palazzolo¹, David J. Peres², Enrico Creaco³, Antonino Cancelliere²

5 ¹Department of Civil Engineering and Architecture, University of Pavia, Italy, now at Department of Civil Engineering and Architecture, University of Catania, Catania, 95123, Italy.

² Department of Civil Engineering and Architecture, University of Catania, Catania, 95123, Italy.

³ Department of Civil Engineering and Architecture, University of Pavia, Pavia, 27100, Italy.

10 *Correspondence to:* Nunziarita Palazzolo (nunziarita.palazzolo@unict.it)

Abstract. In recent times, several efforts have been addressed to understand the extent to which soil moisture estimations may improve the performance of landslide early warning systems (LEWSs). These systems have been traditionally based on rainfall intensity-duration thresholds. Still a limited number of studies explore the possible enhancement of the performance of LEWSs through the identification of hydro-meteorological thresholds. In this study, we propose a methodology for
15 developing regional hydro-meteorological landslide triggering thresholds coupling mean rainfall intensity and soil moisture information. To test the potential improvements in prediction we use ERA5-Land reanalysis soil moisture data, available at four depth levels and hourly resolution. Two different instances are investigated, namely the identification of triggering thresholds using rainfall intensity and the soil moisture at each of four depth levels, and the identification of triggering thresholds using rainfall intensity and a combination of soil moisture at the four depths as obtained by principal component
20 analysis (PCA). We also propose an improvement of the thresholds' parametric form, respect to traditional choices (power law or bi-linear), by using a piece-wise linear equation. The equation's parameters are optimized to maximize the ROC True Skill Statistic (TSS) prediction performance metric. The proposed hydro-meteorological thresholds are tested on the case of Sicily Island (southern Italy) and the performance is compared to that of traditional rainfall intensity-duration (ID) power-law thresholds corresponding to maximum TSS. Overall, the results show that the soil moisture information allows an
25 improvement of prediction performance, as the TSS increases from 0.50 to 0.71, passing from traditional to hydro-meteorological thresholds using soil moisture at the either the first or the second depth level. Using the first principal component, which combines in the most effective way soil moisture the four depth levels, similar performances are obtained. These improvements, gained in spite of the coarse spatial resolution and the limited accuracy of reanalysis data, provide further support to hydro-meteorological thresholds. At the same time, the study shows that the PCA can also be useful for

30 the identification of hydro-meteorological thresholds, as it allows to easily combine multi-layer soil moisture information while keeping the thresholds two-dimensional, and thus easy to be communicated to landslide risk managers.

1 Introduction

The impact of landslides triggered by rainfall is constantly increasing due to landscape modifications, i.e. urbanization, deforestation, land-changes and the abandonment of rural areas (Roccati et al., 2019). Landslides can cause serious damage to man-made structures and land, as well as loss of natural resources and lives. The role of landslide risk in human well-being, is highlighted by the fact that more than 4800 landslide occurrences have been documented from 2004 to 2016, with over 55000 reported fatalities at a global scale (Froude and Petley 2018). Furthermore, landslides triggered by rainfall have been identified as the cause of approximately 90% of fatalities globally (Haque et al. 2016; Sultana 2020) and, from an economic point of view, annual losses were estimated to total USD 20 billion (Sim et al., 2022). In the last decades, an increasing number of studies also focused on the potential effects of climate change on landslide phenomena (McInnes et al. 2007; Dijkstra and Dixon 2010; Crozier 2010), pointing out that there are some unresolved issues, such as the abundance, activity, frequency and return period of landslides in response to the projected climate change (Gariano and Guzzetti, 2016; Peres and Cancelliere, 2018). In light of these considerations and, after recent catastrophic landslides worldwide, there is a high interest of scholars and civil protection agencies in the development of landslide early warning systems (LEWS), which can serve as an aid in predicting possible slope movements, and thus as risk mitigation tool (Roccati et al., 2020; Highland and Bobrowsky, 2008; Chae et al., 2017).

Landslide triggering thresholds are a key component of LEWS. In general, even if LEWS vary widely in approaches and scale, empirical rainfall thresholds in combination with rainfall measurements and forecasts remain the most frequently applied approaches for the majority of regional LEWSs. In the literature, several methods have been proposed for the identification of rainfall thresholds to landslides initiation (Guzzetti et al., 2007a, 2008; Segoni et al., 2018a; Aleotti, 2004). Empirical rainfall thresholds are usually obtained by drawing lower-bound lines to the rainfall conditions inducing landslides, plotted in Cartesian, semi-logarithmic, or logarithmic coordinates (e.g., rainfall duration on the abscissa axis and rainfall intensity on the vertical axis). When information on non-triggering rainfall is also available, thresholds can be determined as the best classifiers based on the confusion matrix (Berti et al., 2012; Staley et al., 2013; Peres and Cancelliere, 2014; Postance et al., 2018; Marino et al., 2020; Peres and Cancelliere, 2021).

Commonly, these rainfall exceedance thresholds empirically relate the occurrence of landslides to rainfall event characteristics such as intensity, duration, total amounts, or a combination thereof (Wicki et al., 2020a). However, in many settings the antecedent soil wetness conditions influence the variability in rainfall triggering amounts, becoming a predisposing factor that plays a major role in landslide initiation (Palau et al., 2021; Conrad et al., 2021). This led to a more recent approach that relies

60 not only on rainfall but, also, on subsurface hydrological measurements (e.g. soil moisture content), thus introducing hydro-
meteorological thresholds (Uwihirwe et al., 2022; Mirus et al., 2018b, a; Thomas et al., 2018; Segoni et al., 2018c; Wicki et
al., 2020a; Bogaard and Greco, 2018, 2016) for a better representation of landslide triggering. The term “hydro-
meteorological” is because these threshold combine a meteorological (rainfall depth) with a hydrological variable (catchment
storage or soil moisture), reflecting the water storage at the catchment or local scale (Gain et al., 2021).

65 In this regard, several attempts aimed at introducing, directly or with models, the effects of soil moisture information in the
empirical thresholds for improving landslide prediction have been made (Crozier, 1999; Zhao et al., 2019; Brocca et al., 2016;
Segoni et al., 2018c; Ponziani et al., 2012). For instance, Marino et al. (2020) performed an explorative numerical investigation
to understand whether soil moisture information can improve shallow landslide forecasting using the hydro-meteorological
threshold approach. In their work, they used synthetic rainfall and landslide data obtained through Monte Carlo simulation.

70 Their results showed that soil moisture information introduced within hydro-meteorological thresholds can significantly reduce
the false alarm ratio of LEWS, while keeping at least unvaried the number of missed alarms. Along this path, Reder and Rianna
(2021) addressed the extent to which soil moisture estimations can be useful to define a proxy for antecedent slope wetness
conditions. In particular, they used the soil moisture data derived from the ERA5-Land reanalysis (Hersbach et al., 2020) as a
support for LEWS, and more specifically as an initial filter for a pre-screening of the effective saturation degree. They showed
75 that the filter yielded by the ERA5 soil model is able to strengthen the regional warning system and that the ERA5 reanalysis
provides estimations consistent with those retrieved by using more complex and detailed physically based models.

Lastly, Wicki et al. (2021) compared the reliability of landslides forecast models based on simulated soil moisture with respect
to models based on soil moisture measurements. Specifically, they assessed the potential and limitations of adopting 1D soil
water transfer model for regional LEWS and disclosed the pros and cons compared of using soil moisture measurements. To
80 this aim, they used plot-scale soil hydrological simulations to be able to directly compare the results to a landslide forecast
model based on in situ soil moisture measurements and demonstrated a high information content of simulated soil moisture
for regional landslide activity, which was even higher than when in situ soil moisture measurements were used (Wicki et al.,
2021). In this regard, Wicki et al. (2020b), demonstrated that the performance is strongly dependent on the distance between
the soil moisture network location and landslide activity area and that the goodness increases with decreasing distances between
85 measurement sites and landslides. Therefore, the density of the soil moisture measurement networks impacts the performance
of a LEWS and these measurement networks should consider the spatial variability of meteorological events and soil properties
(Wicki et al., 2020b).

In light of these advances, in the present work we attempt to give a further contribution by analyzing the possible improvements
of landslide prediction through hydro-meteorological thresholds coupling observed rainfall intensity and soil moisture
90 information, an issue that needs further investigation. In particular, we carry out our investigation considering the ERA5-Land
reanalysis data set. In fact, recent studies proved that the main climate variables (i.e., soil moisture, temperature, precipitation)

obtained from third-generation atmospheric and reanalysis datasets, (i.e., ERA5 project) have a reasonable accuracy in reproducing in situ-measurements of the reference local weather stations from the International Soil Moisture Network (Dorigo et al., 2011; Li et al., 2020; Beck et al., 2021). However, accuracy issues remain still significant, also considering their relatively
95 coarse resolution ($0.1^\circ \times 0.1^\circ \cong 9\text{km}$).

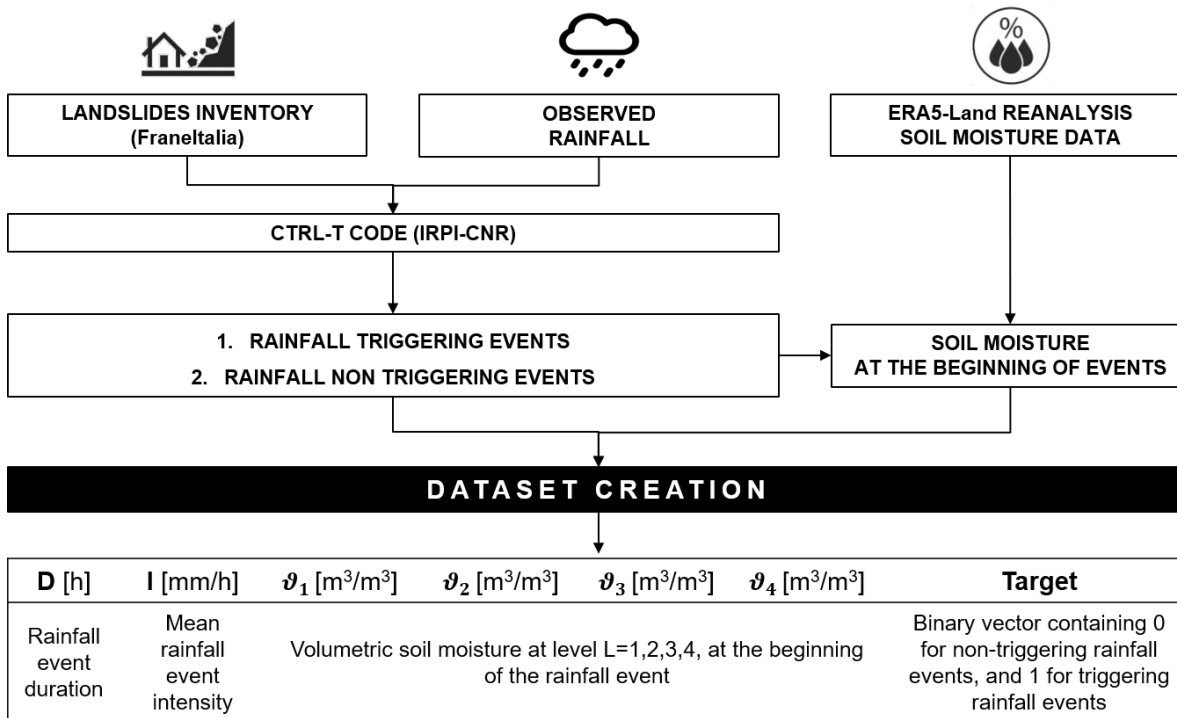
A real case study is used to test the methodology, obtained by joining, over the period 2010-2018, the dataset of observed landslide and rainfall events with the dataset of soil moisture values reconstructed by the ERA5-Land reanalysis at the beginning of rainfall events. The proposed methodology involves the identification of the equation describing the threshold through a heuristic approach and an optimization procedure aimed at finding the optimal values of its parameters, in order to
100 maximize the ROC True Skill Statistic (TSS). In order to combine the information of multiple layers of soil moisture data availability, we explore the use of Principal Component Analysis (PCA) (Jolliffe, 2002), a multivariate statistical tool which capitalizes on the presence of correlation between the soil moisture at different depths. Thus, two different instances are investigated, namely the identification of four triggering thresholds using the rainfall intensity and the soil moisture at each of four depth levels, and the identification of the triggering threshold using the rainfall intensity and first principal component of
105 soil moisture at all four depths.

The paper is organized as follows. First, the procedure for the dataset creation and the methodology leading to the hydro-meteorological thresholds identification are presented in the “Material and Methods” section. Then, the “Study Area” section describes the relevant features of the study area, namely the Sicily Island (Southern Italy). Next, the results and discussion concerning the comparison between the performance obtained through the traditional ID thresholds and the proposed hydro-
110 meteorological thresholds are presented in the “Results and Discussion” section. Finally, conclusions are drawn in the last section.

2 Materials and method

2.1 Dataset construction

The construction of a rainfall and landslide events dataset is a key step that involves different types of data (i.e., observed
115 landslides, rainfall events and, reanalysis data of soil moisture). As schematically illustrated in Fig. 1, in the first step, the FraneItalia project (Calvello and Pecoraro, 2018) is employed to collect information regarding the observed landslides, as it is a thorough spatio-temporal inventory of historical landslides that have impacted the Italian territory since 2010, including both occurrences that resulted in fatalities and occurrences that did not.



120 **Figure 1: Schematization of the procedure followed for dataset construction.**

The first classification criterion by the FraneItalia catalogue is based on the number of landslides triggered by the same rainfall event in a given geographic area. Specifically, single landslide events (SLE) and areal landslide events (ALE) are distinguished for records referring to single or multiple landslides, respectively. Both SLEs and ALEs are then categorized into one of three classes in relation to their impacts, in order to track whether a landslide occurrence resulted in casualties or missing people (C1, very severe), injured people and evacuations (C2, severe), or no one was physically harmed (C3, minor). The data on occurrence location, the date the landslide occurred, the source of information, and the number of landslides for ALEs are further details that have been also included in the catalogue, together with the onset and duration of the landslide occurrence and its consequences.

125 Thanks to this accurate level of detail, it is possible to filter only the landslide events triggered by rainfall, which are precisely those to take into consideration in our study.

The CTRL-T (Calculation of Thresholds for Rainfall-induced Landslides-Tool) code (Melillo et al., 2018) is subsequently used for the identification of the rainfall events that were more likely to be responsible for the observed slope failures. Specifically, CTRL-T automatically and objectively reconstructs rainfall events and the triggering conditions responsible for the failure using a set of adjustable parameters to account for different morphological and climatic settings. Briefly, the tool consists of distinct modules with specific purposes. Among these, one module operates the reconstruction of rainfall events in

term of duration (D , in hours) and, cumulated event rainfall (E , in mm) using continuous hourly rainfall time series and setting several climate and spatial parameters such as, the warm period in a year (C_W); the cold period in a year (C_C); the resolution of the rain gauge (G_S); the instrumental sensitivity of the rain gauge and the minimum value exceeding which the isolated hourly measurements are considered relevant (E_R); and the radius of the buffer to assign each landslide to the closest rain gauge (R_B). Furthermore, in order to account for seasonality (i.e., different evapotranspiration rates in different periods of the year), additional rainfall parameters can be set by the user, namely: the dry interval separating isolated rainfall measurements (P_1); the time periods used to remove irrelevant amounts of rainfall, (P_2), and (P_3); and the minimum dry period separating two rainfall events, (P_4). The readers are referred to Melillo et al., (2018) for more detailed information on these parameters. A further module, instead, performs selection of the rain gauge representative for the landslide. Defined the maximum allowed distance between a landslide and a rain gauge as a circle of radius R_B specified by the user, if more than one rain gauge is located within the circle, the rainfall events from each rain gauge are weighted based on the rain gauge–landslide distance and the rainfall event characteristics (cumulated rainfall and duration). More specifically, given the multiple rainfall conditions (MRC) that are most likely responsible for the slope failures as pair of rainfall event duration (D_L) and cumulated event rainfall (E_L), or a set of two or more pairs, each MRC is assigned a weight to select the representative rain gauge and the rainfall conditions associated with the landslide. The weight is proportional to the inverse square distance between the rain gauge and the landslide (d^{-2}), the cumulated rainfall (E_L), and the rainfall mean intensity ($E_L D_L^{-1}$):

$$w = f(d, E_L, D_L) = d^{-2} E_L^2 D_L^{-1} \quad (1)$$

Thus, among all the identified MRCs, those with the highest weights w are defined as the maximum probability rainfall conditions (MPRCs) and, these reconstructed rainfall conditions were assumed as the triggering rainfall events. Lastly, Fig. 2, depicts how the duration of a triggering rainfall event is defined. Specifically, when a landslide occurs during a dry period the whole event that preceded it is considered as triggering rainfall event; otherwise, just the rainfall that occurred before the landslide occurrence is taken into account.

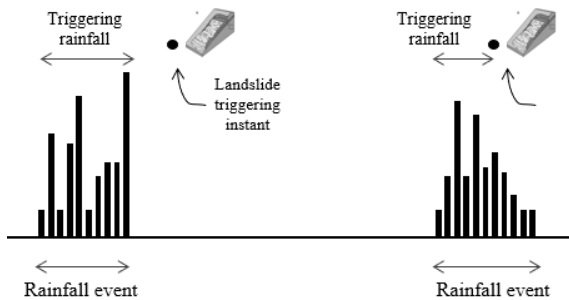


Figure 2: Sketch illustrating how the duration of a triggering rainfall event is defined (adapted from Peres et al., 2018).

160 As shown in Fig. 1, the last step for the dataset set up consists of the association of soil moisture data to the beginning of each rainfall event, both triggering and non-triggering ones. In this regard, the ERA5-Land reanalysis dataset is used. It provides the volume of water ϑ [m^3/m^3] at four distinct soil depths levels (i.e., 0-7 cm; 7-28 cm; 28-100 cm, and 100-289 cm). The ERA5-Land soil moisture data are provided at the hourly scale, as grid data with a horizontal resolution of $0.1^\circ \times 0.1^\circ$. Thus, being at the same temporal resolution of rainfall time series, the soil moisture values representative of the closest cell to the
 165 rain gauge that recorded the rainfall event are associated, without delay, to the considered event. Thereby the dataset in the form shown in Fig. 1 was created.

2.2 Principal component analysis

Principal Component Analysis (Jolliffe, 2002) is a multivariate technique that analyzes a data table in which observations are described by several inter-correlated quantitative dependent variables to extract the important information from the table and
 170 to represent it as a set of new orthogonal variables called principal components (Abdi and Williams, 2010).

Precisely, the data are transformed according to a new coordinate system having the x-axis, known as the first principal axis, characterized by the highest data variation. Along the successive axes (e.g., the second principal axis, the third principal axis, and so on), the data are characterized by increasingly lower variation. Each succeeding principal component explains the maximum amount of variance feasible with the requirement that it is orthogonal to the previous principal components. In
 175 practice, identifying the eigenvalues and eigenvectors of the covariance matrix is the formal mathematical equivalent of solving the PCA problem. The direction along which the data have the highest variance is the eigenvector, while the related eigenvalue is a quantification of the variance in the data along the corresponding eigenvector. Accordingly, the first principal component is the eigenvector with the greatest eigenvalue, followed by the eigenvector with the second-highest eigenvalue, and so on. Thus, the so computed principal components are employed for the projection of the data into the new coordinate space (Kherif
 180 and Latypova, 2019).

Practically, in our study, θ (Eq. 2) represents the soil moisture data table for which to compute the principal components, specified as an n -by- p matrix. Rows correspond the total amount n of the considered rainfall events (i.e., observations), and the number of columns to the four depths levels at which the initial soil moisture data are provided (i.e., variables).

$$\theta = \begin{bmatrix} \vartheta_{11} & \vartheta_{12} & \vartheta_{13} & \vartheta_{14} \\ \vartheta_{21} & \vartheta_{22} & \vartheta_{23} & \vartheta_{24} \\ \vdots & \vdots & \vdots & \vdots \\ \vartheta_{n1} & \vartheta_{n2} & \vartheta_{n3} & \vartheta_{n4} \end{bmatrix} \quad (2)$$

185 A represents, instead, the principal components' loadings (i.e., coefficients) table, specified as an p -by- p matrix. The rows of matrix A are called the eigenvectors, and these specify the orientation of the principal components relative to the original variables.

$$\mathbf{A} = \begin{bmatrix} a_{11} & a_{12} & a_{13} & a_{14} \\ a_{21} & a_{22} & a_{23} & a_{24} \\ a_{31} & a_{32} & a_{33} & a_{34} \\ a_{41} & a_{42} & a_{43} & a_{44} \end{bmatrix} \quad (3)$$

Thus, the principal components (S_i) for the generic i_{th} row are given by a linear combination of the variables θ and \mathbf{A} , namely:

$$190 \quad S_{i1} = a_{11}\vartheta_{i1} + a_{12}\vartheta_{i2} + a_{13}\vartheta_{i3} + a_{14}\vartheta_{i4} \quad (4)$$

$$S_{i2} = a_{21}\vartheta_{i1} + a_{22}\vartheta_{i2} + a_{23}\vartheta_{i3} + a_{24}\vartheta_{i4} \quad (5)$$

$$S_{i3} = a_{31}\vartheta_{i1} + a_{32}\vartheta_{i2} + a_{33}\vartheta_{i3} + a_{34}\vartheta_{i4} \quad (6)$$

$$S_{i4} = a_{41}\vartheta_{i1} + a_{42}\vartheta_{i2} + a_{43}\vartheta_{i3} + a_{44}\vartheta_{i4} \quad (7)$$

with $i = 1, \dots, n$.

195 In matrix notation, the transformation of the original variables to the principal components is written as,

$$\mathbf{S} = \theta \mathbf{A} \quad (8)$$

2.3 Threshold identification

The methodology adopted in this work aims to improve the identification of regional landslides triggering thresholds by means of reanalysis soil moisture information and to compare the obtained performance with those obtained through the traditional rainfall intensity-duration power-law thresholds (ID). Therefore, the rainfall intensity-duration threshold, the most common type of threshold proposed and adopted in the literature (Segoni et al., 2018b; Guzzetti et al., 2007b; Brunetti et al., 2010), is used as benchmark. The ID threshold assumes the form $I = \alpha D^{-\beta}$, where I [mm/h] represents the rainfall intensity, i.e., the average precipitation rate over the considered period; D [h] represents the duration of the rainfall event; α is the intercept parameter, and β is the slope parameter. After reconstructing the rainfall events with the methodology explained for the dataset creation and, after calculating the main variables (i.e., mean rainfall intensity and duration), an optimization tool (i.e., the MATLAB® Particle Swarm optimization toolbox) is used with the aim to search for the best possible α and β curve parameters able to maximize the True Skill Statistic index (TSS) objective function (Eq. 11), which is based on the confusion matrix or the Receiver-Operating Characteristics (ROCs). The confusion matrix is expressed in terms of the count of true positives (TP), true negatives (TN), false positives (FP) and false negatives (FN) (Peirce, 1884) (Table 1).

210

Table 1: Confusion matrix for ROC analysis.

		Observed landslide	
		Landslide (P)	No landslide (N)
Predicted Landslide	Landslide	TP	FP
	No landslide	FN	TN

As a function of the variables reported in Table 1, the three reference standard ROC indices – namely, True Positive Rate, False Positive Rate and True Skill Statistic – are listed below (Eqs. 9, 10, 11):

$$\text{TPR} = \frac{\text{TP}}{(\text{TP} + \text{FN})} \quad (9)$$

$$215 \quad \text{FPR} = \frac{\text{FP}}{(\text{TN} + \text{FP})} \quad (10)$$

$$\text{TSS} = \text{TPR} - \text{FPR} \quad (11)$$

The highest performances correspond to $\text{TSS} = 1$, when, the model produces no false or missing predictions.

Afterward, the analysis is focused on the identification of the parametric equation that represents the lower boundary between triggering and non-triggering rainfall events on the basis of the mean rainfall intensity and the reanalysis of soil moisture values at each depth level. In this context, we propose the following parametric threshold as a reliable relationship to classify the events on the semi-log plane:

$$I = \begin{cases} y_0, & \vartheta < x_0 \\ \frac{y_1 - y_0}{x_1 - x_0} (\vartheta - x_0) + y_0, & x_0 \leq \vartheta \leq x_1 \\ y_1, & \vartheta > x_1 \end{cases} \quad (12)$$

where I and ϑ correspond to rainfall intensity and to soil moisture values, respectively. This parametric form of the threshold has been devised based on the visual inspection of the scatter plot of triggering and non-triggering events (i.e., heuristically), and corroborated by comparison with other relationships proposed in the literature – specifically, the power-law and the simple bilinear (as opposed to a linear or more complex power or high-degree polynomial) (Uwihirwe et al., 2022; Thomas et al., 2019; Mirus et al., 2018a). x_0, x_1, y_0 , and y_1 are the threshold's parameters that must be estimated. In this regard, these parameters are computed by adopting the same objective function and optimization procedure as those used for the identification of the parameters of the power-law ID threshold, i.e., the TSS objective function (Eq. 11) and the MATLAB® Particle Swarm global optimization toolbox. At this stage, the threshold identification methodology described so far is applied with the aim to identify triggering thresholds between the mean rainfall intensity (I) and the soil moisture expressed in two variants: *i*) soil moisture at each of the four depth levels ($\vartheta_1, \vartheta_2, \vartheta_3, \vartheta_4$) available from the ERA 5 - reanalysis; *ii*) the first principal component of soil moisture, i.e. the linear combination of soil moisture at the four depths corresponding to the minimum information loss (highest explained variance). The TSS values obtained in the applications considering soil moisture (hereinafter indicated as TSS_{par}) were compared with the TSS values obtained for the reference scenario of the power-law ID threshold (hereinafter TSS_{pl}).

3 Study area

The study area selected for our study is the island of Sicily (southern Italy, 37.75N-14.25 E) which, with an area of ~25,700 km², is the largest island of the Mediterranean Sea. A hilly morphology (62%) dominates the landscape in the island, while the rest is characterized by a mountainous and flat morphology, especially in the eastern part of the island around Catania. The terrain average elevation is about 400 meters above sea level, ranging from 0 to 3320 meters on the peak of the Etna volcano. Geologically, the Sicily Island arose during the Neogene, when the European and African plates converged. Thus, Sicily stands out for its complex geological and lithological features which, cooperatively with anthropic activities (e.g., changes in land use, management of forest, etc.), have generated a wide range of different types of soil (Venturella, 2004).

The climate is warm-temperate, with hot and dry summers, especially on the southern coasts, and higher and more frequent precipitation during the colder winter months, in the mountainous internal areas (Pumo et al., 2019). Mean annual precipitation ranges between 700 and 800 mm and, autumn and winter are the rainiest seasons. The most severe rainfall events frequently hit the eastern side of the island and specifically, the eastern side of the Etna volcano and the flanks of the Peloritani Mountains, with the greatest precipitation peaks on the Ionian side (Gariano et al., 2015). On the other hand, south Sicily is distinguished by lower precipitation than the mean values recorded in the rest of the region, since it is located at a lower height and is exposed to the hot and dry African winds (Alecci and Rossi, 2007).

Fig. 3 shows the geographical context of Sicily, the rain gauge locations for the period 2009-2018 (Distefano et al., 2021) and the observed landslide locations. In more detail, 207 landslide events were retrieved by the FraneItalia database from 2010 to 2018 and, for each of them, longitude-latitude coordinates (WGS84 datum), together with the initiation time, are retrieved.

255

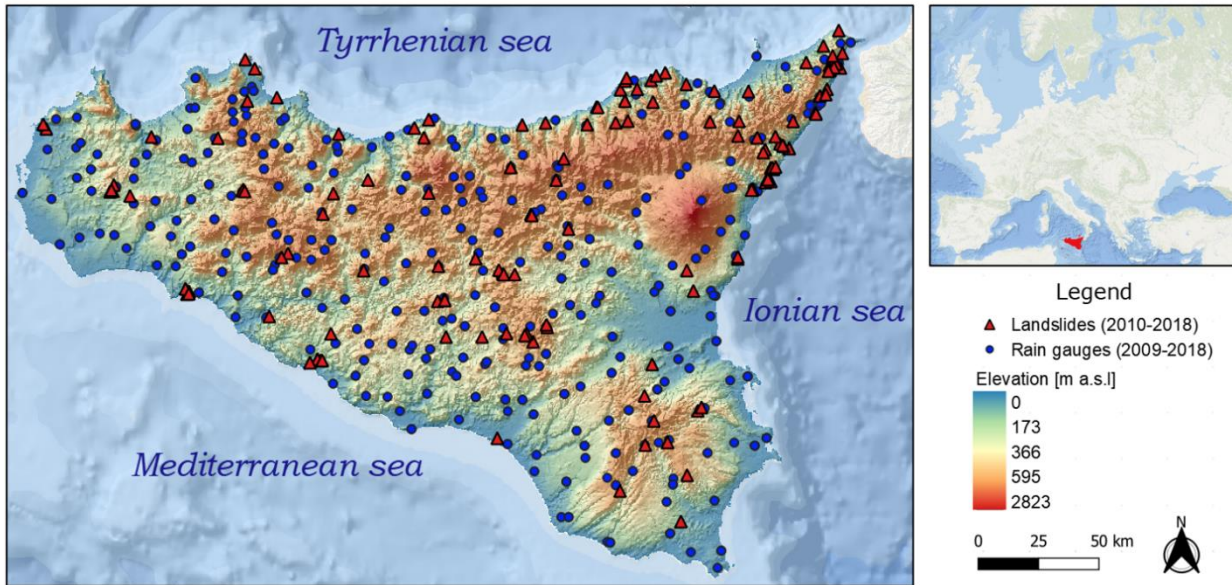


Figure 3: Elevation map of the study area (Sicily region), showing the location of the rain gauges and landslide occurrences. (Credit to: <http://www.sinanet.isprambiente.it/it/sia-ispra/download-mais> and ESRI 2020).

Concerning the observed rainfall measurements, we consulted the data provided by the regional water observatory (Osservatorio delle Acque, OdA), the SIAS (Sicilian Agro-meteorological Information Service), and the Regional Civil Protection Department (DRPC), namely the three main gauging networks installed in Sicily.

This enabled an hourly time series to be reconstructed for the precipitation over the period 2009-2018. As previously explained in Section 2.1, using these continuous rainfall time series, the rainfall events were identified using the CTRL-T research code. For the calibration of these regional parameters required by CTRL-T, we referred to a previous application of the algorithm to the Sicily Island (Melillo et al., 2015). Specifically, according to this approach, the dry period (no rain) has been set equal to 48 hours ($P_{4, \text{warm}}$) between April and October (warm season, C_w), while it has been set equal to 96 hours ($P_{4, \text{cold}}$) from November to March (cold season, C_c). Indeed, in line with Köppen (1931) and Trewartha (1968), it is reasonable to assume that in Sicily, due to the Mediterranean climate, the warm period is longer than the cold one. The rain gauge sensitivity G_S has set equal to 0.2 mm, while the rain gauge search radius R_B has been established equal to 16 km. Table 2 summarizes adopted values for mentioned CTRL-T parameters.

Table 2: CTRL-T parameters for the reconstruction of the rainfall events used in the present study.

G_S [mm]	E_R [mm]	R_B [km]	P_1 [h]		P_2 [h]		P_3 [h]		P_4 [h]	
			C_w	C_c	C_w	C_c	C_w	C_c	C_w	C_c
0.2	0.2	16	3	6	6	12	1	1	48	96

4 Results and discussion

4.1 Principal Component Analysis

275 An explorative analysis was carried out, to investigate the correlation between the four soil moisture depths ($\vartheta_1, \vartheta_2, \vartheta_3, \vartheta_4$).
The plot shown in Fig. 4 represents the correlation matrix between all pairs of variables, together with the Pearson's correlation coefficients.

Overall, all the four soil moisture depths are related to each other. Specifically, the diagonal subplot between the upper two depths levels ϑ_1 and ϑ_2 has the highest correlation with a Pearson correlation coefficient equal to 0.85. This suggest that PCA can be adopted in order to find out the linear combination expressing the correlation between the involved soil moisture
280 variables.

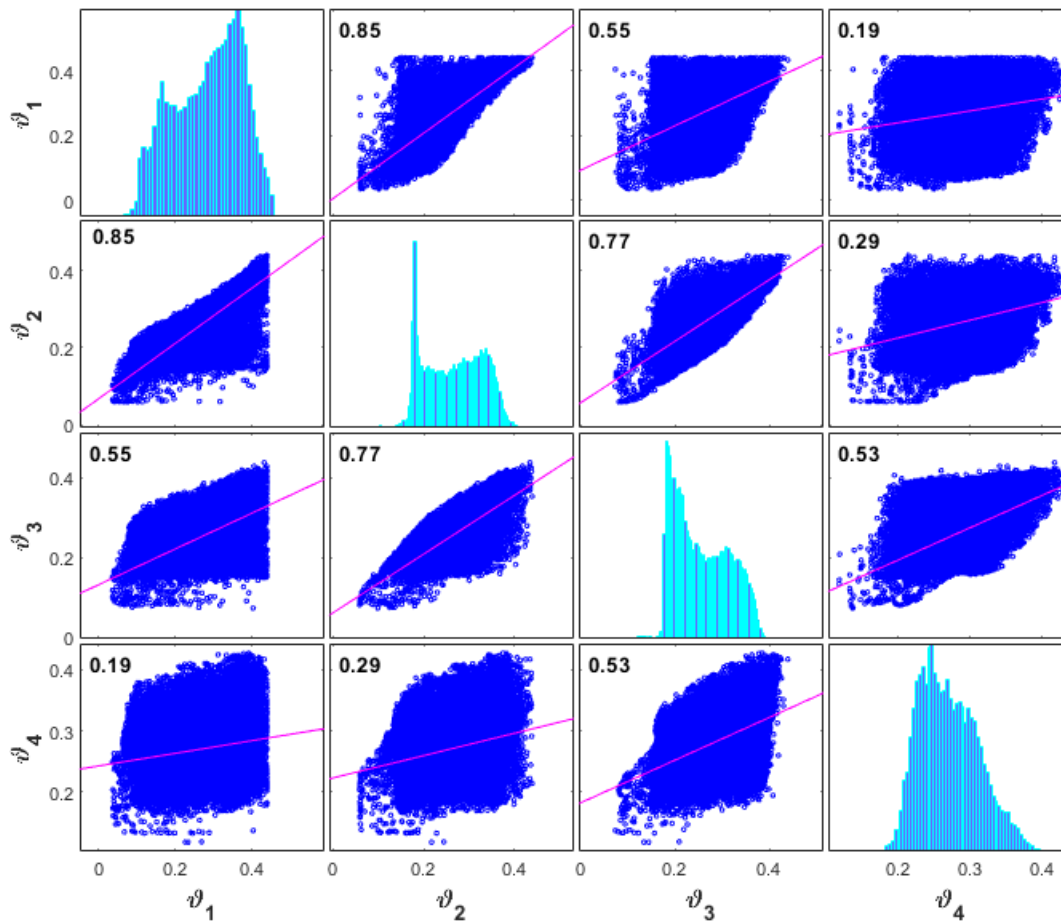


Figure 4: Correlation matrix between the four soil moisture level depths ($\vartheta_1, \vartheta_2, \vartheta_3, \vartheta_4$). Each off-diagonal subplot contains a scatterplot of a pair of variables with a least-squares reference line, the slope of which is equal to the displayed Pearson correlation coefficient. Each diagonal subplot contains the distribution of a variable as a histogram.

285 The preliminary step, required when PCA is performed, is to center the data on the mean values of each variable, namely by subtracting the mean. This step allows the cloud of data to be centered on the origin of the principal components, but it affects neither the spatial relationships of the data, nor the explained variance along the variables. At this stage, it was possible to proceed with PCA and, according to Eqs. 4, 5, 6, and 7, the four principal components of soil moisture were defined as follow:

$$S_{i1} = 0.65\vartheta_{i1} + 0.58\vartheta_{i2} + 0.47\vartheta_{i3} + 0.15\vartheta_{i4} \quad (13)$$

290 $S_{i2} = -0.54\vartheta_{i1} - 0.04\vartheta_{i2} + 0.63\vartheta_{i3} + 0.55\vartheta_{i4} \quad (14)$

$$S_{i3} = 0.37\vartheta_{i1} - 0.29\vartheta_{i2} - 0.39\vartheta_{i3} + 0.79\vartheta_{i4} \quad (15)$$

$$S_{i4} = -0.38\vartheta_{i1} + 0.76\vartheta_{i2} - 0.48\vartheta_{i3} + 0.23\vartheta_{i4} \quad (16)$$

The loadings values of each principal component are intended as the weights a_{ij} (Eq. 3): therefore, the higher the value of the weight, the larger the contribution of a variable to the component associated with the weight. The sign of a loading indicates whether a variable and a principal component are positively or negatively correlated. Here, although overall slightly large loadings correspond to the first principal component, none of the four variables has a strong relationship with a particular principal component.

295

Fig. 5(a) shows the scree plot representing the total percentage of variance explained by each of the four principal components. The chart reveals the decreasing rate at which variance is explained by additional principal components. Fig. 5(b) represents a grouped bar plot indicating the estimated loadings corresponding to each of four principal components as reported at Eqs. 13, 14, 15, and 16.

300

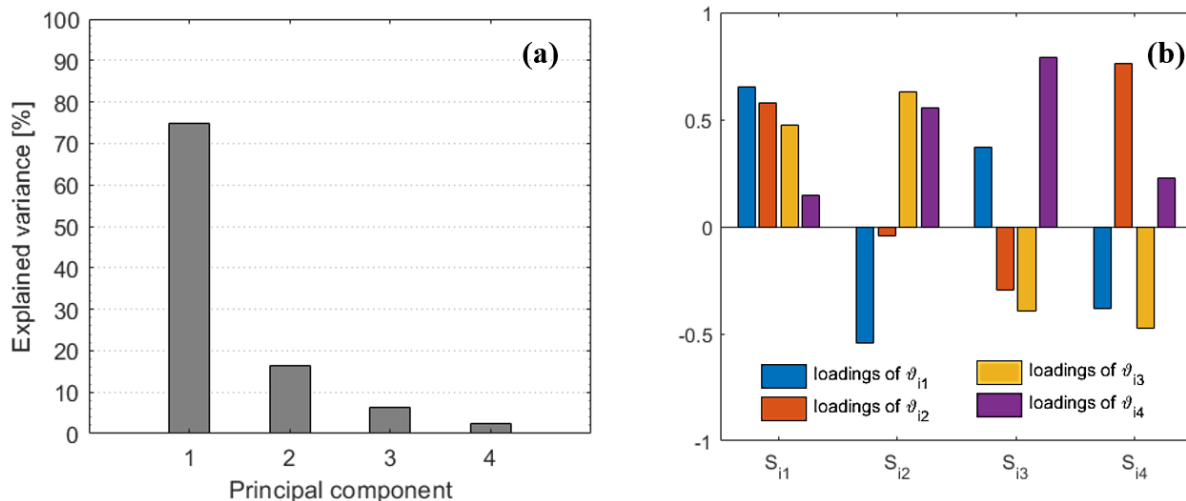


Figure 5: (a) Total variance explained by each principal component; (b) Estimated loadings for each principal component S_i .

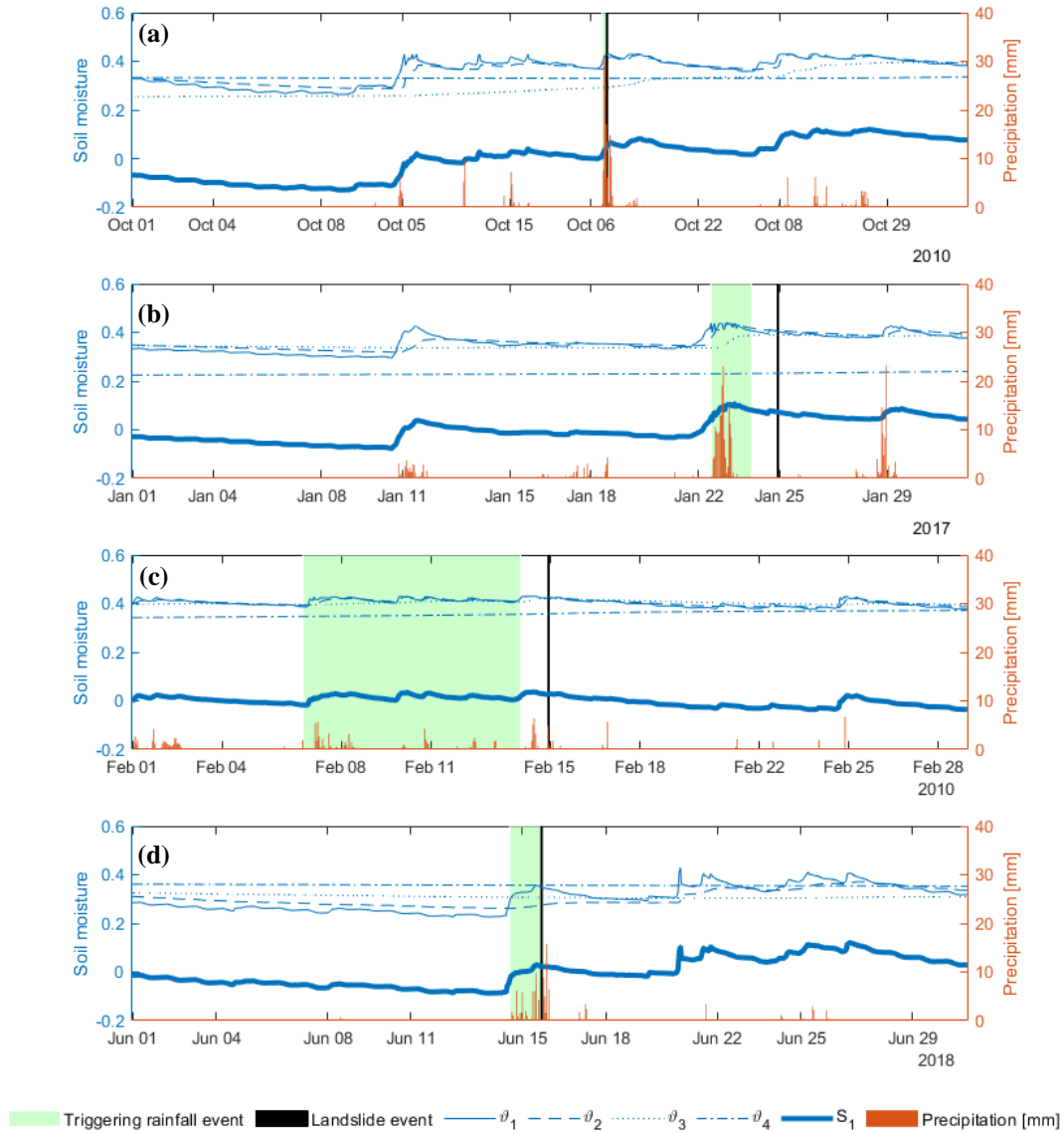
Because dimensionality reduction is a goal of PCA, several criteria can be considered for determining how many principal components should be examined and how many should be ignored (Rencher, 1998). Just to list a few: *i*) ignore principal

305

components at the point at which the next principal component offers little increase in the total explained variation; *ii*) ignore the last principal component whose explained variation are all roughly equal; *iii*) include all principal components up to a predetermined total explained variation. In our study, the third criterion was applied considering a threshold value of 75%. Therefore, only the first principal component was considered as it guaranteed the desired explained variation of about 75 %.

310 **4.2 Thresholds identification**

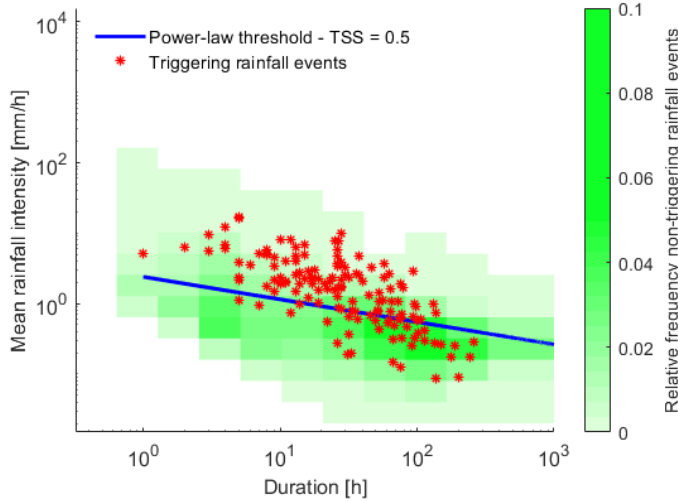
CTRL-T tool reconstructed 144 landslide events out of the 207 landslides retrieved by the FraneItalia database. Four different triggering rainfall events, representing a range of triggering conditions, were selected within the database, and the precipitation time series together with the soil moisture time series are plotted in Fig. 6.



315 **Figure 6:** Panel showing four different triggering rainfall events. For each of them the precipitation time series together with the soil
 moisture time series ($\vartheta_1, \vartheta_2, \vartheta_3, \vartheta_4$) are reported, as well as the first principal component of soil moisture S_1 and the timing of each
 320 landslide.

As expected, the upper two soil moisture layers are those that are most similar to precipitation trends, as well as the first
 principal component of soil moisture S_1 , computed using Eq. 13. Overall, a greater variability in soil moisture values can be
 320 observed in correspondence to ϑ_1 and ϑ_2 , which assume maximum values about equal to 0.4 in correspondence of all the
 analyzed triggering rainfall events.

First, the power-law ID threshold maximizing TSS was identified (Fig. 7). In particular, the plot shows the triggering events as red points, while the non-triggering, since there are in a very large number, are better represented by a colormap indicating the relative frequency of non-triggering rainfall events, following a plotting technique inspired to Leonarduzzi et al. (2017).



325

Figure 7: Traditional power-law threshold on the log-log plane between observed mean rainfall intensity (I) and duration (D).

For this threshold a $TSS_{pl} = 0.50$, corresponding to a $TPR_{pl} = 0.76$ and $FPR_{pl} = 0.26$, is obtained, and this value was taken as benchmark for comparison to the hydro-meteorological thresholds. Fig. 8 shows the obtained thresholds when the mean rainfall intensity and the soil moisture at each of the four depth levels are considered. As can be seen, especially in
 330 correspondence to the upper two depths (i.e., 0-7 cm, 7-28 cm), the triggering rainfall events are located, for the most, on the right-upper side of the graph, suggesting that the equation proposed for the identification of the thresholds (Eq. 12) fits this trend well. Furthermore, at all depths taken into consideration, there is a noticeable clustering of the highest relative frequency values of non-triggering rainfall events below the related parametric threshold. All four identified thresholds have better performance than ID threshold. Specifically, higher TSS values were obtained for the first two depths, with a TSS_{par} equal to
 335 0.71, while significantly lower values of TSS_{par} (0.61 and 0.54) are obtained with the third and fourth soil moisture level, respectively.

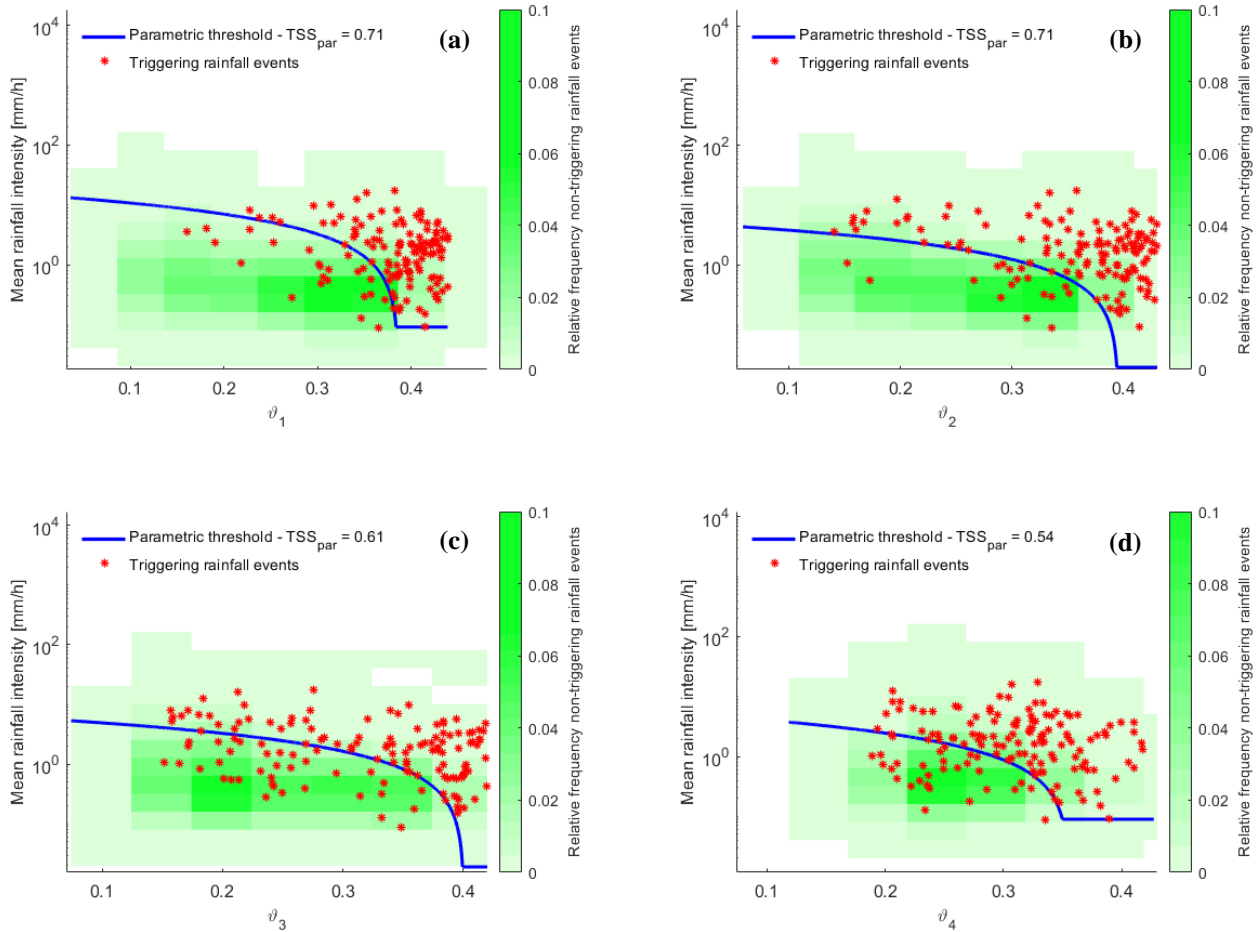
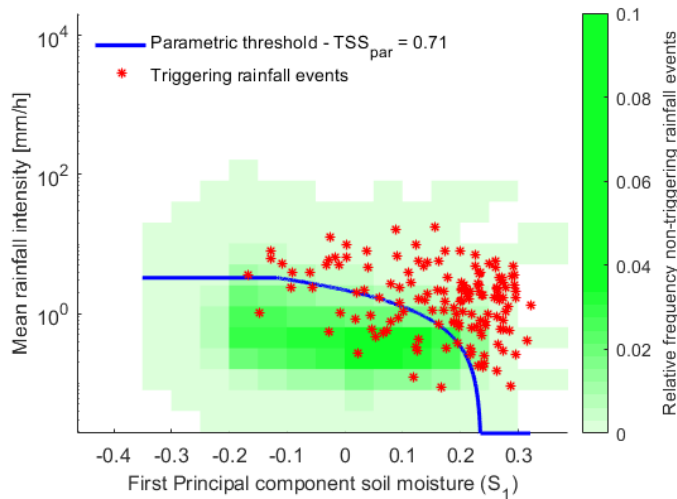


Figure 8: Parametric thresholds on the semi-log plane between mean rainfall intensity and soil moisture at the four distinct depths: (a) ϑ_1 0-7 cm; (b) ϑ_2 7-28 cm; (c) ϑ_3 28-100 cm; (d) ϑ_4 100-289 cm.

340 As previously mentioned, the second analysis concerns the identification of the optimal parametric thresholds when the mean rainfall intensity and first principal component of soil moisture are considered (Fig. 9). In this case, a $TSS_{par} = 0.71$ was obtained once again.



345 **Figure 9: Parametric threshold on the semi-log plane between observed mean rainfall intensity (I) and first principal component of soil moisture (S_1).**

Table 3 summarizes the TSS values in correspondence of the analyzed thresholds, together with the values of parameters (Eq. 12) estimated for the parametric thresholds.

Table 3: TSS values in correspondence to each analyzed scenario, and parameters (x_0, y_0, x_1, y_1) estimated for the parametric thresholds.

Parametric threshold	TPR_{par}	FPR_{par}	TSS_{par}	x_0	y_0	x_1	y_1
$I\theta_1$	0.84	0.14	0.71	-0.33	27.23	0.38	0.09
$I\theta_2$	0.84	0.14	0.71	0.05	5.73	0.39	0.02
$I\theta_3$	0.73	0.12	0.61	-0.03	6.98	0.40	0.02
$I\theta_4$	0.79	0.25	0.54	-0.08	6.82	0.35	0.09
IS_1	0.85	0.14	0.71	-0.12	3.28	0.23	0.02

350

Overall, the proposed hydro-meteorological thresholds proved able to better predict the landslide occurrences when compared to the performance of the traditional ID approach.

355 For the specific case study of Sicily Island, thus the use of PCA has no significant advantages in terms of prediction performance. Nevertheless, PCA still remains a valid approach to combining the information of the four available layers and can be applied to avoid the trial-and-error testing of the use of the various single layers, as the performances are at least as good. At the same time, this calls for further investigations about the possible increase in performances thanks to the

combination of multi-layered information in a single variable through PCA. These investigations may involve other case study areas (different climates and quality of the landslide and rainfall datasets), as well as more specific analyses focused, for instance, on landslide type, seasonality, etc., which are out of the scope of the present work, given also the lack of the needed data. The parametric form proposed in this work in Eq. (12) was also compared with other more traditional ones. Taking as reference variables the observed mean rainfall intensity (I) and first principal component of soil moisture (S_1), it proved to be better than the power-law threshold within the log-log plane and to the bi-linear threshold within the semi-log plane, which scored lower values of TSS , equal to 0.51 and 0.66, respectively. This highlights the importance of defining thresholds using an adequate parametric equation, as this choice can limit the exploitation of soil moisture information for improving their prediction performance.

5 Conclusions

In this study, the potential improvements of regional landslide prediction by the use of soil moisture information and multivariate statistical analysis (PCA) were explored, with reference to the case study of Sicily, Italy. For the investigation, we have used ERA5-Land reanalysis soil moisture information. The hydro-meteorological thresholds, combining precipitation and soil moisture information, proved better at classifying triggering and non-triggering rainfall events when compared to the traditional ID power-law thresholds. Specifically, a valuable improvement was found when the upper layers of soil moisture are used for the hydro-meteorological threshold identification, leading to TSS_{par} values up to 0.71, which were much higher than those obtained with the traditional approach (i.e., $TSS_{pl} = 0.50$). Moreover, the application of the PCA to soil moisture data at various depths enables by-passing the problem of identifying the most influential soil layer on landslide triggering, without deteriorating significantly performance and keeping the thresholds simple (two-dimensional). In real situations, the use of the reanalysis data is limited by the fact that they are made available to the public with a delay of some weeks from present. This delay is expected to be significantly reduced in the near future, in light of the increasing computational capabilities. Finally, our study corroborates with real data the potential improvements of the prediction capabilities of landslide triggering thresholds that use soil moisture information, which can be even greater with more accurate in-situ distributed soil moisture measurements. In this regard, the appreciable improvements obtained despite the inherent uncertainty of the reanalysis global dataset, further encourages the identification of the hydro-meteorological thresholds using surface soil moisture products with enhanced spatial and temporal resolution (i.e., in situ measurements, reanalysis and satellite soil moisture data provided at real or near real time). Future developments of the work will consider other regions in order to investigate more in depth the potentialities of PCA in improving landslide prediction performance, also by taking into account further information on landslides - e.g., spatial patterns, landslides properties, seasonality - not easily available for the region considered in this study.

Authors' contributions. Conceptualization, N.P., D.J.P., E.C. and A.C.; formal analysis, N.P. and D.J.P.; investigation, N.P. and D.J.P.; methodology, N.P. and D.J.P.; coding, N.P. and D.J.P.; supervision, D.J.P., E.C. and A.C.; writing original draft, N.P. and D.J.P.; writing, review and editing, N.P., D.J.P., E.C. and A.C. All authors have read and agreed to the published
390 version of the manuscript.

Data availability. FraneItalia landslides catalogue (Calvello and Pecoraro, 2018) is available at <https://franeitalia.wordpress.com/database/> (last accessed on 16/06/2022). Rainfall measurements are available at websites of the Servizio Informativo Agrometeorologico Siciliano (SIAS) (<http://www.sias.regione.sicilia.it/>, last accessed on 16/06/2022) and at the Osservatorio delle Acque (<http://www.acq.isprambiente.it/annalipdf/>, ISPRA, 2020 – for Sicily, last accessed on
395 16/06/2022). Reanalysis soil moisture data are available from <https://cds.climate.copernicus.eu/cdsapp#!/dataset/reanalysis-era5-land?tab=form> (last accessed on 16/06/2022).

Acknowledgements. Nunziarita Palazzolo doctoral program's grant was funded by University of Pavia, and she is supported by post-doctoral contract "Eventi idrologici estremi e resilienza ai cambiamenti climatici", funded within the activities of the research project "LIFE SimetoRES - Urban adaption and community learning for a RESilient Simeto Valley" - Grant
400 Agreement n. LIFE17 CCA/IT/000115 - CUP C65H18000550006. Research partially carried out within the project HydrEx – Hydrological extremes in a changing climate – Piano di incentivi per la ricerca di Ateneo (Pia.ce.ri.), 2020-2022, Università di Catania. APCs funded by “Fondi di Ateneo 2020-2022, Università di Catania, linea Open Access”.

References

Abdi, H. and Williams, L. J.: Principal component analysis, Wiley Interdiscip. Rev. Comput. Stat., 2, 433–459,
405 <https://doi.org/10.1002/WICS.101>, 2010.

Alecci, S. and Rossi, G.: Controllo di qualità dei dati pluviometrici ed analisi delle serie temporali, Siccità. Anal. Monit. e mitigazione. Appl. Sicil. Nuova Ed. Bios, Cosenza, Ital., 2007.

Aleotti, P.: A warning system for rainfall-induced shallow failures, Eng. Geol., 73, 247–265,
<https://doi.org/10.1016/j.enggeo.2004.01.007>, 2004.

410 Beck, H. E., Pan, M., Miralles, D. G., Reichle, R. H., Dorigo, W. A., Hahn, S., Sheffield, J., Karthikeyan, L., Balsamo, G., Parinussa, R. M., van Dijk, A. I. J. M., Du, J., Kimball, J. S., Vergopolan, N., and Wood, E. F.: Evaluation of 18 satellite- And model-based soil moisture products using in situ measurements from 826 sensors, Hydrol. Earth Syst. Sci., 25, 17–40,
<https://doi.org/10.5194/hess-25-17-2021>, 2021.

- Berti, M., Martina, M. L. V., Franceschini, S., Pignone, S., Simoni, A., and Pizziolo, M.: Probabilistic rainfall thresholds for landslide occurrence using a Bayesian approach, *J. Geophys. Res. Earth Surf.*, 117, 1–20, <https://doi.org/10.1029/2012JF002367>, 2012.
- Bogaard, T. and Greco, R.: Invited perspectives: Hydrological perspectives on precipitation intensity-duration thresholds for landslide initiation: Proposing hydro-meteorological thresholds, *Nat. Hazards Earth Syst. Sci.*, 18, 31–39, <https://doi.org/10.5194/nhess-18-31-2018>, 2018.
- 420 Bogaard, T. A. and Greco, R.: Landslide hydrology: from hydrology to pore pressure, *Wiley Interdiscip. Rev. Water*, 3, 439–459, <https://doi.org/10.1002/wat2.1126>, 2016.
- Brocca, L., Ciabatta, L., Moramarco, T., Ponziani, F., Berni, N., and Wagner, W.: Use of Satellite Soil Moisture Products for the Operational Mitigation of Landslides Risk in Central Italy, Elsevier Inc., 231–247 pp., <https://doi.org/10.1016/B978-0-12-803388-3.00012-7>, 2016.
- 425 Brunetti, M. T., Peruccacci, S., Rossi, M., Luciani, S., Valigi, D., and Guzzetti, F.: Rainfall thresholds for the possible occurrence of landslides in Italy, *Nat. Hazards Earth Syst. Sci.*, 10, 447–458, <https://doi.org/10.5194/nhess-10-447-2010>, 2010.
- Calvello, M. and Pecoraro, G.: FraneItalia: a catalog of recent Italian landslides, 5, <https://doi.org/10.1186/s40677-018-0105-5>, 2018.
- Chae, B.-G., Park, H.-J., Catani, F., Simoni, A., and Berti, M.: Landslide prediction, monitoring and early warning: a concise review of state-of-the-art, 21, 1033–1070, <https://doi.org/10.1007/s12303-017-0034-4>, 2017.
- 430 Coe, J. A. and Godt, J. W.: Review of approaches for assessing the impact of climate change on landslide hazards, in: *Landslides and Engineered Slopes: Protecting Society through Improved Understanding - Proceedings of the 11th International and 2nd North American Symposium on Landslides and Engineered Slopes*, 2012, 371–377, 2012.
- Conrad, J. L., Morphew, M. D., Baum, R. L., and Mirus, B. B.: HydroMet: A new code for automated objective optimization of hydrometeorological thresholds for landslide initiation, 13, <https://doi.org/10.3390/w13131752>, 2021.
- 435 Crozier, M. J.: Prediction of rainfall-triggered landslides: a test of the Antecedent Water Status Model, *Earth Surf. Process. Landforms*, 24, 825–833, [https://doi.org/10.1002/\(SICI\)1096-9837\(199908\)24:9<825::AID-ESP14>3.0.CO;2-M](https://doi.org/10.1002/(SICI)1096-9837(199908)24:9<825::AID-ESP14>3.0.CO;2-M), 1999.

- Crozier, M. J.: Deciphering the effect of climate change on landslide activity: A review, 124, 260–267, 440 <https://doi.org/10.1016/J.GEOMORPH.2010.04.009>, 2010.
- Dijkstra, T. A. and Dixon, N.: Climate change and slope stability in the UK: challenges and approaches, *Q. J. Eng. Geol. Hydrogeol.*, 43, 371–385, <https://doi.org/10.1144/1470-9236/09-036>, 2010.
- Distefano, P., Peres, D. J., Scandura, P., and Cancelliere, A.: Brief communication: Rainfall thresholds based on Artificial neural networks can improve landslide early warning, <https://doi.org/10.5194/nhess-2021-206>, 2021.
- 445 Dorigo, W. A., Wagner, W., Hohensinn, R., Hahn, S., Paulik, C., Xaver, A., Gruber, A., Drusch, M., Mecklenburg, S., Van Oevelen, P., Robock, A., and Jackson, T.: The International Soil Moisture Network: A data hosting facility for global in situ soil moisture measurements, *Hydrol. Earth Syst. Sci.*, 15, 1675–1698, <https://doi.org/10.5194/hess-15-1675-2011>, 2011.
- Froude, M. J. and Petley, D. N.: Global fatal landslide occurrence from 2004 to 2016, *Nat. Hazards Earth Syst. Sci.*, 18, 2161–2181, <https://doi.org/10.5194/nhess-18-2161-2018>, 2018.
- 450 Gain, A. K., Bühler, Y., Haegeli, P., Molinari, D., Parise, M., Peres, D. J., Pinto, J. G., Trigo, R. M., Llasat, M. C., and Kreibich, H.: Brief Communication : Key papers of 20 years in Natural Hazards and Earth System Sciences, 1–13, 2021.
- Gariano, S. L. and Guzzetti, F.: Landslides in a changing climate, *Earth-Science Rev.*, 162, 227–252, <https://doi.org/10.1016/J.EARSCIREV.2016.08.011>, 2016.
- Gariano, S. L., Brunetti, M. T., Iovine, G., Melillo, M., Peruccacci, S., Terranova, O., Vennari, C., and Guzzetti, F.: Calibration 455 and validation of rainfall thresholds for shallow landslide forecasting in Sicily, southern Italy, 228, 653–665, <https://doi.org/10.1016/j.geomorph.2014.10.019>, 2015.
- Guzzetti, F., Peruccacci, S., Rossi, M., and Stark, C. P.: Rainfall thresholds for the initiation of landslides in central and southern Europe, *Meteorol. Atmos. Phys.*, 98, 239–267, <https://doi.org/10.1007/s00703-007-0262-7>, 2007a.
- Guzzetti, F., Peruccacci, S., Rossi, M., and Stark, C. P.: Rainfall thresholds for the initiation of landslides in central and 460 southern Europe, *Meteorol. Atmos. Phys.*, 98, 239–267, <https://doi.org/10.1007/s00703-007-0262-7>, 2007b.
- Guzzetti, F., Peruccacci, S., Rossi, M., and Stark, C. P.: The rainfall intensity-duration control of shallow landslides and debris flows: An update, 5, 3–17, <https://doi.org/10.1007/s10346-007-0112-1>, 2008.

- Hersbach, H., Bell, B., Berrisford, P., Hirahara, S., Horányi, A., Muñoz-Sabater, J., Nicolas, J., Peubey, C., Radu, R., Schepers, D., Simmons, A., Soci, C., Abdalla, S., Abellan, X., Balsamo, G., Bechtold, P., Biavati, G., Bidlot, J., Bonavita, M., De Chiara, G., Dahlgren, P., Dee, D., Diamantakis, M., Dragani, R., Flemming, J., Forbes, R., Fuentes, M., Geer, A., Haimberger, L., Healy, S., Hogan, R. J., Hólm, E., Janisková, M., Keeley, S., Laloyaux, P., Lopez, P., Lupu, C., Radnoti, G., de Rosnay, P., Rozum, I., Vamborg, F., Villaume, S., and Thépaut, J. N.: The ERA5 global reanalysis, *Q. J. R. Meteorol. Soc.*, 146, 1999–2049, <https://doi.org/10.1002/qj.3803>, 2020.
- Highland, L. M. and Bobrowsky, P.: The landslide Handbook - A guide to understanding landslides, *US Geol. Surv. Circ.*, 1–147, <https://doi.org/10.3133/cir1325>, 2008.
- Jolliffe, I. T.: Principal component analysis for special types of data, Springer New York, (pp. 338-372). pp., 2002.
- Kherif, F. and Latypova, A.: Principal component analysis, *Mach. Learn. Methods Appl. to Brain Disord.*, 209–225, <https://doi.org/10.1016/B978-0-12-815739-8.00012-2>, 2019.
- Koppen, V. P.: Das geographische System der Klimate, in: *Hand- buch der Klimatologie*, edited by: Köppen, W. and Geiger, R., Berlin, Gebrüder Bornträger, Band 5, Teil C, 44 pp., 1936 (in German).
- Leonarduzzi, E., Molnar, P., and McArdell, B. W.: Predictive performance of rainfall thresholds for shallow landslides in Switzerland from gridded daily data, *Water Resour. Res.*, 53, 6612– 6625, doi:10.1002/2017WR021044, 2017.
- Li, M., Wu, P., and Ma, Z.: A comprehensive evaluation of soil moisture and soil temperature from third-generation atmospheric and land reanalysis data sets, *Int. J. Climatol.*, 40, 5744–5766, <https://doi.org/10.1002/joc.6549>, 2020.
- Marino, P., Peres, D. J., Cancelliere, A., Greco, R., and Bogaard, T. A.: Soil moisture information can improve shallow landslide forecasting using the hydrometeorological threshold approach, 17, 2041–2054, <https://doi.org/10.1007/s10346-020-01420-8>, 2020.
- McInnes, R., Jakeways, J., Fairbank, H., and Mathie, E.: Landslides and Climate Change: Challenges and Solutions: Proceedings of the International Conference on Landslides and Climate Change, Ventnor, Isle of Wight, UK, 21-24 May 2007, CRC Press, 2007.
- Melillo, M., Brunetti, M. T., Peruccacci, S., Gariano, S. L., and Guzzetti, F.: An algorithm for the objective reconstruction of rainfall events responsible for landslides, *Landslides*, 12, 311–320, <https://doi.org/10.1007/s10346-014-0471-3>, 2015.
- Melillo, M., Brunetti, M. T., Peruccacci, S., Gariano, S. L., Roccati, A., and Guzzetti, F.: A tool for the automatic calculation

- of rainfall thresholds for landslide occurrence, *Environ. Model. Softw.*, 105, 230–243, 490 <https://doi.org/10.1016/j.envsoft.2018.03.024>, 2018.
- Mirus, B. B., Morphew, M. D., and Smith, J. B.: Developing Hydro-Meteorological Thresholds for Shallow Landslide Initiation and Early Warning, *Water* 2018, Vol. 10, Page 1274, 10, 1274, <https://doi.org/10.3390/W10091274>, 2018a.
- Mirus, B. B., Becker, R. E., Baum, R. L., and Smith, J. B.: Integrating real-time subsurface hydrologic monitoring with empirical rainfall thresholds to improve landslide early warning, 15, 1909–1919, <https://doi.org/10.1007/s10346-018-0995-z>, 495 2018b.
- Palau, R. M., Hürlimann, M., Berenguer, M., and Sempere-Torres, D.: Towards the use of hydrometeorological thresholds for the regional-scale LEWS of Catalonia (NE Spain)., <https://doi.org/10.5194/EGUSPHERE-EGU21-8221>, 2021.
- Peirce, C. S.: The numerical measure of the success of predictions., *Science*, 4, 453–454, <https://doi.org/10.1126/science.ns-4.93.453-a>, 1884.
- 500 Peres, D. J. and Cancelliere, A.: Derivation and evaluation of landslide-triggering thresholds by a Monte Carlo approach, *Hydrol. Earth Syst. Sci.*, 18, 4913–4931, <https://doi.org/10.5194/hess-18-4913-2014>, 2014.
- Peres, D. J. and Cancelliere, A.: Modeling impacts of climate change on return period of landslide triggering, *J. Hydrol.*, 567, 420–434, <https://doi.org/10.1016/j.jhydrol.2018.10.036>, 2018.
- Peres, D. J. and Cancelliere, A.: Comparing methods for determining landslide early warning thresholds: potential use of non-triggering rainfall for locations with scarce landslide data availability, 18, 3135–3147, <https://doi.org/10.1007/s10346-021-01704-7>, 2021. 505
- Ponziani, F., Pandolfo, C., Stelluti, M., Berni, N., Brocca, L., and Moramarco, T.: Assessment of rainfall thresholds and soil moisture modeling for operational hydrogeological risk prevention in the Umbria region (central Italy), 9, 229–237, <https://doi.org/10.1007/s10346-011-0287-3>, 2012.
- 510 Postance, B., Hillier, J., Dijkstra, T., and Dixon, N.: Comparing threshold definition techniques for rainfall-induced landslides: A national assessment using radar rainfall, *Earth Surf. Process. Landforms*, 43, 553–560, <https://doi.org/10.1002/ESP.4202>, 2018.
- Pumo, D., Carlino, G., Blenkinsop, S., Arnone, E., Fowler, H., and Noto, L. V.: Sensitivity of extreme rainfall to temperature

in semi-arid Mediterranean regions, *Atmos. Res.*, 225, 30–44, <https://doi.org/10.1016/j.atmosres.2019.03.036>, 2019.

- 515 Reder, A. and Rianna, G.: Exploring ERA5 reanalysis potentialities for supporting landslide investigations: a test case from Campania Region (Southern Italy), 18, 1909–1924, <https://doi.org/10.1007/S10346-020-01610-4>, 2021.

Rencher, A. C.: *Multivariate statistical inference and applications*, Wiley-Interscience, 1998.

- Roccati, A., Faccini, F., Luino, F., Ciampalini, A., and Turconi, L.: Heavy rainfall triggering shallow landslides: A susceptibility assessment by a GIS-approach in a Ligurian Apennine catchment (Italy), 11, <https://doi.org/10.3390/w11030605>,
520 2019.

Roccati, A., Paliaga, G., Luino, F., Faccini, F., and Turconi, L.: Rainfall threshold for shallow landslides initiation and analysis of long-term rainfall trends in a mediterranean area, <https://doi.org/10.3390/atmos11121367>, 2020.

Segoni, S., Piciullo, L., and Gariano, S. L.: A review of the recent literature on rainfall thresholds for landslide occurrence, <https://doi.org/10.1007/s10346-018-0966-4>, 1 August 2018a.

- 525 Segoni, S., Piciullo, L., and Gariano, S. L.: A review of the recent literature on rainfall thresholds for landslide occurrence, 15, 1483–1501, <https://doi.org/10.1007/s10346-018-0966-4>, 2018b.

Segoni, S., Rosi, A., Lagomarsino, D., Fanti, R., and Casagli, N.: Brief communication: Using averaged soil moisture estimates to improve the performances of a regional-scale landslide early warning system, *Nat. Hazards Earth Syst. Sci.*, 18, 807–812, <https://doi.org/10.5194/NHESS-18-807-2018>, 2018c.

- 530 Sim, K. Ben, Lee, M. L., and Wong, S. Y.: A review of landslide acceptable risk and tolerable risk, <https://doi.org/10.1186/s40677-022-00205-6>, 2022.

Staley, D. M., Kean, J. W., Cannon, S. H., Schmidt, K. M., and Laber, J. L.: Objective definition of rainfall intensity-duration thresholds for the initiation of post-fire debris flows in southern California, 10, 547–562, <https://doi.org/10.1007/s10346-012-0341-9>, 2013.

- 535 Thomas, M. A., Mirus, B. B., and Collins, B. D.: Identifying Physics-Based Thresholds for Rainfall-Induced Landsliding, *Geophys. Res. Lett.*, 45, 9651–9661, <https://doi.org/10.1029/2018GL079662>, 2018.

Thomas, M. A., Collins, B. D., and Mirus, B. B.: Assessing the Feasibility of Satellite-Based Thresholds for Hydrologically

Driven Landsliding, *Water Resour. Res.*, 55, 9006–9023, <https://doi.org/10.1029/2019WR025577>, 2019.

Trewartha, G. T.: *An introduction to climate*, 4th edn., McGraw- Hill, New York, 408 pp., 1968.

540 Uwihirwe, J., Riveros, A., Wanjala, H., Schellekens, J., Sperna Weiland, F., Hrachowitz, M., and Bogaard, T. A.: Potential of satellite-derived hydro-meteorological information for landslide initiation thresholds in Rwanda, *Nat. Hazards Earth Syst. Sci.*, 22, 3641–3661, <https://doi.org/10.5194/nhess-22-3641-2022>, 2022

Venturella, G.: Climatic and pedological features of Sicily, 17, 47–53, 2004.

545 Wicki, A., Lehmann, P., Hauck, C., Seneviratne, S. I., Waldner, P., and Stähli, M.: Assessing the potential of soil moisture measurements for regional landslide early warning, 17, 1881–1896, <https://doi.org/10.1007/s10346-020-01400-y>, 2020a.

Wicki, A., Lehmann, P., Hauck, C., Seneviratne, S. I., Waldner, P., and Stähli, M.: Assessing the potential of soil moisture measurements for regional landslide early warning, 17, 1881–1896, <https://doi.org/10.1007/S10346-020-01400-Y/>, 2020b.

550 Wicki, A., Jansson, E., Lehmann, P., Hauck, C., and Stähli, M.: Simulated or measured soil moisture: which one is adding more value to regional landslide early warning?, *Hydrol. Earth Syst. Sci.*, 25, 4585–4610, <https://doi.org/10.5194/hess-25-4585-2021>, 2021.

Zhao, B., Dai, Q., Han, D., Dai, H., Mao, J., and Zhuo, L.: Probabilistic thresholds for landslides warning by integrating soil moisture conditions with rainfall thresholds, *J. Hydrol.*, 574, 276–287, <https://doi.org/10.1016/j.jhydrol.2019.04.062>, 2019.